# Morphology Control in Water of Polyion Complex Nanoarchitectures of Double-Hydrophilic Charged Block Copolymers through Composition Tuning and Thermal Treatment

**ARTICLE** *in* MACROMOLECULES · APRIL 2014

Impact Factor: 5.8 · DOI: 10.1021/ma500314d



**7 AUTHORS**, INCLUDING:

Yasutaka Anraku
The University of Tokyo
**18** PUBLICATIONS **418** CITATIONS
SEE PROFILE

Akihiro Kishimura
Kyushu University
**49** PUBLICATIONS **1,371** CITATIONS
SEE PROFILE

Kazunori Kataoka
The University of Tokyo
**688** PUBLICATIONS **37,549** CITATIONS
SEE PROFILE

Macromolecules

Article

pubs.acs.org/Macromolecules

# Morphology Control in Water of Polyion Complex Nanoarchitectures of Double-Hydrophilic Charged Block Copolymers through Composition Tuning and Thermal Treatment

Arie Wibowo,[†,§] Kensuke Osada,[†,‡,§] Hiroyuki Matsuda,[†] Yasutaka Anraku,[†] Haruko Hirose,[⊥] Akihiro Kishimura,[∥,⊥,*] and Kazunori Kataoka[†,#,*]

[†]Graduate School of Engineering, The University of Tokyo, 7-3-1, Hongo, Bunkyo-ku, Tokyo, 113-8656, Japan

[‡]Japan Science and Technology Agency, PRESTO, 4-1-8 Honcho, Kawaguchi, Saitama 332-0012, Japan

[⊥]Teijin Ltd.,4-3-2, Asahigaoka, Hino, Tokyo,191-8512, Japan

[∥]Center for Molecular Systems, and [⊥]Department of Applied Chemistry, Faculty of Engineering, Kyushu University, 744 Moto-oka, Nishi-ku, Fukuoka, 819-0395, Japan

[#]Graduate School of Medicine, The University of Tokyo, 7-3-1, Hongo, Bunkyo-ku, Tokyo, 113-8655, Japan

Supporting Information

**ABSTRACT:** Polyion complexes (PICs) are attractive as eco-friendly materials, because they offer simple and fast preparation methods to exert various functionalities in aqueous medium. However, control of nanoarchitectures in PIC materials has not been fully realized, except for the case of micelles and unilamellar vesicles formed from block ionomers. Here, the procedure to control PIC nanoarchitectures with various morphologies was established for the first time by careful tuning in the composition of PICs made from PEG-based block-ionomers with a varying amount of homoionomers as additive to modulate the PEG weight fraction ($f_{PEG}$) in the obtained PICs. Accordingly, the variation in $f_{PEG}$ from 12.1% to 6.5% induced vigorous transition in the microphase separated structures of PICs basically from micelle to lamella via cylindrical network. Notably, uniformed lamella with alternative layers of PEG and PIC domains was found at elevated temperature (70 °C), which, by lowering temperature, reversibly transformed to cylindrical PIC network apparently with connected aqueous channel in mesoscopic scale.

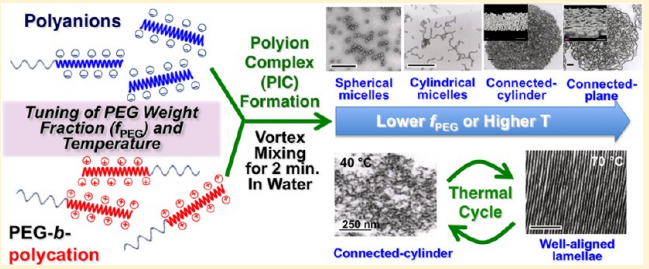


## 1. INTRODUCTION

New materials based on self-assembly of block copolymers finds wide application in many areas because their morphology, size, and function can be precisely controlled by tuning the properties of the polymeric components, in terms of molecular weight, primary structure, secondary structure, and blending ratio for the polymer mixtures.[1−4] However, the method to precisely regulate nanoarchitectures in self-assembled structures of block copolymer is still a challenge especially in aqueous medium even though there is a strong demand from ecological and biomedical viewpoints. In this regard, polyion complexes (PICs) are quite attractive, because they form spontaneously in aqueous medium from an oppositely charged pair of polyelectrolytes without any cumbersome processes.[5−19] There have been several approaches to regulate the nanoarchitectures of PIC materials, but the only limited examples include micelles[12−14,18,19] and unilamellar PIC vesicles termed as "PICsomes"[15−17] prepared from a system containing PEG-based charged block copolymers. Apparently, segregation between PEG and PIC phase drives the formation of these nanoarchitectures as in the case with microphase separation in AB block copolymers in selective solvents. Worth noting is that the transition from PIC micelles to PICsomes in these examples has a strong correlation with the weight fraction of poly(ethylene glycol) (PEG) in the entire polymer system ($f_{PEG}$).[18,19] Polymeric micelles were formed at high $f_{PEG}$ composition (≥10%), and might be transformed into unilamellar polymeric vesicles when $f_{PEG}$ is decreased, by either detachment of PEG part,[18] or by increasing ionic segment in the PEG-based block aniomers.[19] Nevertheless, these structures may not yet constitute as the complete set of all possible nanoarchitectures, because modern theory of AB diblock copolymer based on the mean-field approach actually predicts the existence of other structures in between sphere and lamellar structures,[20,21] which, to the best of our knowledge, have not been thoroughly explored for PIC system. Considering that we have already found polymeric micelles and unilamellar polymeric vesicles for the PIC system, other

Received: February 10, 2014
Revised: April 23, 2014

   dx.doi.org/10.1021/ma500314d | Macromolecules XXXX, XXX, XXX−XXX

PIC nanoarchitectures might be highly expected to be located in between these distinct micelles and lamellar assembly, which were probably achievable by a more careful fine-tuning of their $f_{PEG}$ composition. To this end, there are basically three methods to change the $f_{PEG}$, namely by modulating chain length of PEG segment, modulating chain length of ionomers segment, and modulating PEG composition ratio by blending homopolymers replacing the block copolymers. In this study, we chose the blending method because this method allowed precise control of $f_{PEG}$ by simply changing the blending ratio. Herein, we report successful formation of various PIC nanoarchitectures in aqueous medium with physiological salt concentration (150 mM NaCl), by careful modulation of polymer composition, particularly $f_{PEG}$, and incubation temperature.

## 2. EXPERIMENTAL SECTION

**Materials.** Several types of polyelectrolytes that were used in this work can be seen in Scheme 1a. The cationic block copolymer, PEG-*b*-poly([5-aminopentyl]-*α*,*β*-aspartamide) (PEG−P(Asp-AP); $M_n$ of PEG = 2k, DP of P(Asp-AP) = 84), anionic block copolymer, PEG-*b*-poly(*α*,*β*-aspartic acid) (PEG−PAsp; $M_n$ of PEG = 2k, DP of PAsp = 85), and anionic homopolymer, poly(*α*,*β*-aspartic acid) (homo-PAsp; DP of PAsp = 69) were synthesized as described previously.[16] Glutaraldehyde (GA) was purchased from Wako Pure Chemical Industries, Ltd. (Tokyo, Japan). Carbon-coated 400 mesh copper grids were purchased from Nissin EM (Tokyo, Japan).

**Scheme 1. (a) Chemical Structures of Polymers Used in This Study and (b) Schematic Representation of PIC Preparation**

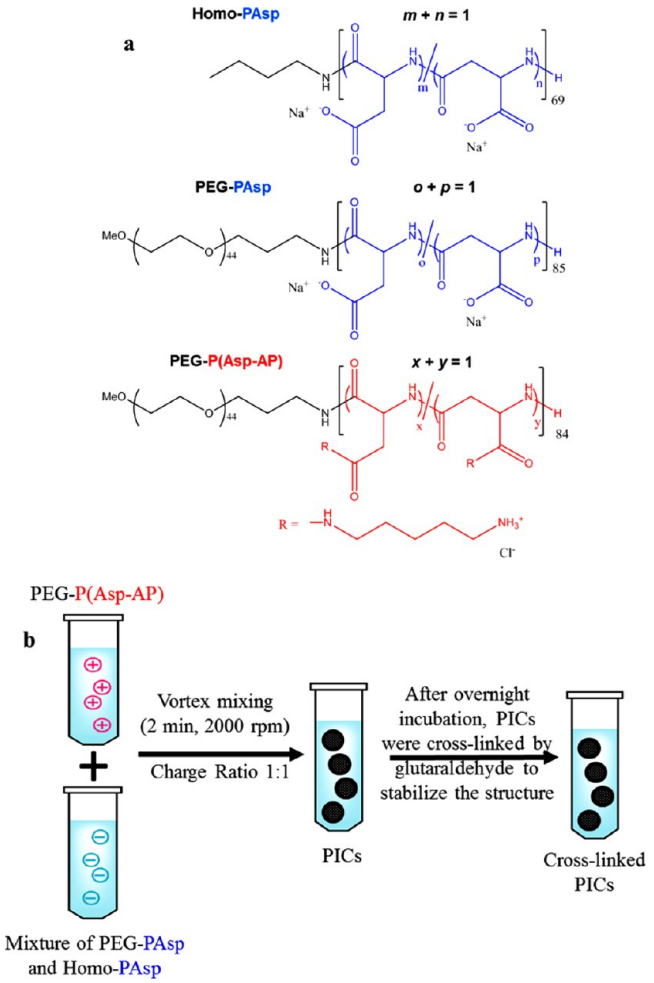


**General Preparation of PICs.** First, all the polymers were separately dissolved in 4-(2-hydroxyethyl)-1-piperazineethanesulfonic acid (HEPES) buffer (10 mM, pH 7.4, 150 mM NaCl). Buffer solutions of PEG−PAsp and homo-PAsp were blended with designated ratio, and then the resulting polyanion mixture was mixed with PEG−P(Asp-AP) in an equal charge unit ratio of $-COO^-$ and $-NH_3^+$ to form PICs (Scheme 1b). After keeping PIC solution overnight with expectation that the structure of PICs had been already reached in equilibrium as the PIC nanoarchitectures did not significantly changed after 2 h of the preparation, an excess amount of GA solution was added to fix the structure of PICs subsequent to the morphology analysis of PICs.

**Preparation of PICs at Different Incubation Temperature.** Before mixing, pretreatment were conducted by storing all of the polymer solutions at designated temperature for 10 min. Solution of the polyanion mixture consist of PEG−PAsp and homo-PAsp was added to the PEG−P(Asp-AP) solution in an equal charge unit ratio of $-COO^-$ and $-NH_3^+$, followed by 2,000 rpm vortex mixing for 2 min, to give PICs. Subsequently, PIC solution was incubated in a controlled temperature condition using a thermostatic bath (SM-05R, Taitec Corporation, Japan). After overnight incubation, an excess amount of GA solution was added to PIC solution, followed by gentle mixing more than 2 h. To check reversibility of thermoresponsive properties of PICs, two times cycle incubation of PICs at 40 and 70 °C was conducted. After that, an excess amount of GA solution was added to each sample, followed by gentle mixing more than 2 h.

**Preparation of Cross-Sectioned Specimens.** The PICs fixed by GA were postfixed in 2% $OsO_4$, dehydrated in a graded series of alcohol and embedded in EPON 812 (TAAB Laboratories, U.K.). The epoxy resin block was then ultramicrotomed by a diamond knife at room temperature using a Sorvall Porter-Blum MT-2 ultramicrotome. The ultrathin section was transferred onto a Cu mesh grid. Prior to the transmission electron microscopy (TEM) and 3D observations by TEM tomography, the ultrathin section was double stained by uranyl acetate for 10 min and lead citrate for 2 min.

**Transmission Electron Microscopy (TEM).** Morphologies of PICs were observed by TEM on H-7000 electron microscope (Hitachi Ltd., Japan) operating at 75 kV. To observe morphology of polymeric micelles, one $\mu$L of the sample solution was placed onto carbon-coated 400 mesh copper grid (Nisshin EM, Japan), that was previously glow-discharged by Eiko IB-3 ion coater (Eiko Engineering Co.Ltd., Japan). Samples were stained by deposition of a drop of a 50% ethanol solution containing 2 wt % uranyl acetate onto the surface of the sample-loaded grid and dried at room temperature. The nanostructures inside the micrometer droplets were observed from the ultrathin sectioned specimen. The obtained TEM images were analyzed with ImageJ software to measure average PIC thickness and spacing between PIC layers.

**3-D TEM Tomography.** Acquisition of tilt series for TEM tomography was performed on a JEM-2100F electron microscope (JEOL, Ltd., Japan) with a ZrO/W(100) electron gun operated at 200 kV. The transmitted images were obtained using a CCD camera (Ultrascan US4000) in the TEM mode, and micrographs with 4k × 4k pixel elements were acquired at tilt angles ranging from −65° to +65° in 1° increments. The alignment of the data series was done with TEMography software (System in Frontier, Inc., Tokyo, Japan). Obtained tomography images were analyzed using TRI/3D-BON software (Ratoc System Engineering Co. Ltd., Japan).

## 3. RESULTS AND DISCUSSIONS

### 3.1. The Influence of $f_{PEG}$ on PIC Nanoarchitectures.

Three types of polyelectrolytes (PEG−PAsp, PEG−P(Asp-AP) and homo-PAsp; Scheme 1a) were used for controlling $f_{PEG}$ values, by which their values could be predicted by simply changing the blending ratio of PEG−PAsp and homo-PAsp (*b*:*h* ratio). Afterward, a series of sample with polymer concentration 1 mg/mL were prepared at 25 °C by varying


dx.doi.org/10.1021/ma500314d | Macromolecules XXXX, XXX, XXX−XXX

**Table 1. TEM Image Analysis of PICs Prepared at Room Temperature (25 °C) with Varying Polymer Composition at a Concentration of 1 mg/mL**

| blending ratio (b/h ratio) | $f_{PEG}$ (%) | apparent morphology observed in TEM | average PIC diameter/thickness determined by TEM (nm) |
|---|---|---|---|
| 10:0 | 12.1 | spherical micelles (Figure 1a) | 20.1 ± 2.9 |
| 8:2 | 11.1 | spherical micelles (Figure 1b) | 20.0 ± 3.8 |
| 6:4 | 10.0 | mixture of spherical and cylindrical micelles (Figure 1c) | spherical, 18.1 ± 4.2; short axis, 12.4 ± 1.7; long axis, 239.2 ± 91.0 |
| 5:5 | 9.4 | network texture (connected-cylinder; Figure 2a) | 12.7 ± 1.7 |
| 4:6 | 8.8 | network texture (connected-cylinder; Figure 2b) | 12.4 ± 1.3 |
| 2:8 | 7.7 | network texture (connected-plane; Figure 2c) | 13.7 ± 1.5 |
| 0:10 | 6.5 | network texture (connected-plane; Figure 2d) | 16.0 ± 2.0 |

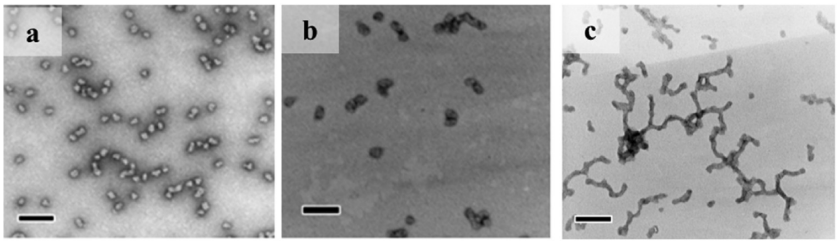


**Figure 1.** TEM images of PICs (scale bars represent 100 nm) obtained at room temperature (25 °C) and polymer concentration 1 mg/mL with $f_{PEG}$ (a) 12.1%, (b) 11.1%, and (c) 10.0%.

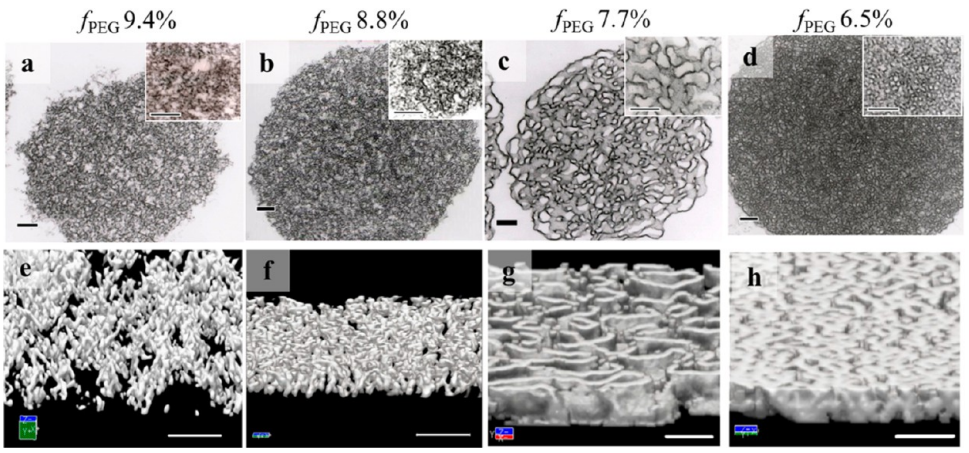


**Figure 2.** Detailed structural analysis carried out by cross-section TEM (a–d; scale bars represent 250 nm) and 3D TEM tomography (e–h; analyzed by 3D-BON software; scale bars represent 100 nm) of PICs obtained at room temperature (25 °C) and polymer concentration 1 mg/mL with $f_{PEG}$ 9.4%–6.5%. Inset images of parts a–d are cross-section TEM images for each micrometer-sized particle that were taken at higher magnification. Movies of 3D-TEM results are available as a Supporting Information.

their $b/h$ ratio allowing for variation of $f_{PEG}$ from 6.5 to 12.1% (Table 1) to identify the influence of $f_{PEG}$ on PIC nanoarchitectures.

At high $f_{PEG}$ composition ($f_{PEG}$ 12.1 and 11.1%), resulting PIC solution appeared to be transparent, and dynamic light scattering (DLS) results showed the formation of particles with sizes ranging from 40–50 nm (Table S1, Supporting Information). Transmission electron microscopy (TEM) observations revealed the particles to be spherical with diameter ~20 nm (Table 1, Figure 1a,b). As these features are consistent to polymeric micelles, thus the observed spherical particles is reasonable to assume as PIC micelles as reported previously.[12,14,18] Slight decrease in PEG weight fraction ($f_{PEG}$ composition 10.0%) also gave transparent solution and the TEM observation showed spherical structure together with cylindrical structures (Figure 1c), where the former (18.1 ± 4.2 nm) with a diameter similar to the one obtained at $f_{PEG}$ = 12.1 and 11.1% (20.1 ± 2.9 and 20.0 ± 3.8 nm respectively) and the latter with a short axis of 12.4 ± 1.7 nm with substantially distributed long axis length (239.2 ± 91.0 nm; Table 1), implying shift from spherical polymeric micelles to cylindrical polymeric micelles with decrease of $f_{PEG}$. Upon further lowering the $f_{PEG}$ (≤9.4%), resulting PIC solutions appeared to be turbid, and particle size determination by electrical sensing zone method showed the formation of micrometer-sized objects with sizes ranging from 2–5 μm (Table S2). The micrometer-sized droplets was indeed confirmed by optical microscopic observations performed by dark-field and phase-contrast microscopies (DFM and PCM, respectively; Figure S1), therefore distinct transition from polymeric micelles to micrometer-sized droplets was observed to occur at this $f_{PEG}$.

Given the immiscible nature of PEG and PIC part, it is wondering if the PICs settle homogeneously or in segregated form within the micrometer-sized particles. With this regard, further characterizations were carried out on their cross-section sample to find out their possible PIC structure within the


dx.doi.org/10.1021/ma500314d | Macromolecules XXXX, XXX, XXX–XXX

micrometer-sized droplets by TEM. To this end, the cross-sectioned specimen was prepared from the resin embedded PICs. As a pretreatment, the PICs were fixed by a cross-linking agent, in which GA was used as it is recognized to elicit less influence in the structures, and frequently used to fix the structures of cells, biological tissues[22−25] and also enzyme immobilization.[26,27] To further confirm GA fixing process did not affect the PIC structures, we also investigated another cross-linking reagent, which has different cross-linking mechanism, given an assumption that if the PIC structures were enough sensitive to the reaction, the PIC structures would be different between two fixing agents. Under this assumption, the PICs were fixed by GA and 1-ethyl-3-(3-(dimethylamino)-propyl)carbodiimide (EDC), and the obtained cross-sectioned specimens were observed by TEM. Consequently, essentially the same structures were observed for the GA- and EDC-cross-linked samples at the corresponded PEG weight fraction ($f_{PEG}$) (Figure S2), suggesting that the influence of the fixing process was insignificant on the PIC structures.

Cross-section TEM observation displayed porous architectures in the micrometer-sized PIC droplets (Figure 2a−d). Note that the PIC domains are stained in black due to strong affinity of staining agents (uranyl acetate and lead citrate) to PIC part, while hydrated PEG is not visible due to lower affinity of PEG to the staining agents. The network architectures may look somewhat different in PICs of $f_{PEG}$ = 9.4%, 8.8% (Figure 2a,b), and $f_{PEG}$ = 7.7%, 6.5% (Figure 2c,d). To get further detailed information on these nanoarchitectures of PICs, three-dimensional (3D) TEM tomography analysis was carried out (Figures 2e−h and S3−S6 and movies in the Supporting Information). Three dimensional (3D) tomography results showed that there seemed two different network structures of PICs. The first one was observed at $f_{PEG}$ = 9.4% and 8.8% presenting element looked like cylinders connecting each other (Figures 2e,f and S3 and S4; Supporting Information, Movies S1 and S2), thus named here as "connected-cylinder PIC network". TEM image analysis showed that the average PIC thickness was 12.4 ± 1.3 nm, which is quite similar to short axis length of the cylindrical polymeric micelles observed at $f_{PEG}$ = 10.0% (12.4 ± 1.7 nm) (Table 1). The second one was observed at $f_{PEG}$ = 7.7% and 6.5%, presenting elements looked like plane continuously connecting each other (Figure 2g-h, S5 and S6; Supporting Information, Movies S3 and S4), thus termed by "connected-plane PIC network". Worth mentioning is that the averaged thicknesses of the PIC plane measured from TEM image (13.7 ± 1.5 nm and 16.0 ± 2.0 nm for $f_{PEG}$ = 7.7% and 6.5%, respectively: Table 1) are analogous to the thickness of PIC lamellar of previously reported unilamellar PIC vesicles (10−15 nm).[16] This analogy of PIC thickness may allow assuming the observed PIC plane is consisted of unilamellar of PIC. Given the length of constituent polyelectrolytes in fully extended confirmation is calculated to be 20.2 nm for P(Asp-AP) segment in PEG−P(Asp-AP) (DP of P(Asp-AP) = 84), 20.4 nm for PAsp segment in PEG−PAsp (DP of PAsp = 85) and 16.6 nm for homo-PAsp chain (DP of PAsp =69) (calculated from the average backbone unit, C−C−N = 0.24 nm), the assumption that the observed PIC plane to be unilamellar may be within acceptable range.

Consequently, upon decreasing $f_{PEG}$ of PICs by replacing PEG−PAsp to PAsp, we found significant morphological change from spherical polymeric micelle to cylindrical polymeric micelle, and finally to micrometer-sized particle retaining fine textures characterized as segregated PIC network as seen in Figure 2. This trend may present analogy of microphase segregation pattern modeled for AB diblock copolymer system, namely sphere−cylinder−bicontinuous-lamella,[2,3,20,21] if compromising assumptions of the observed connected networks as bicontinuous phase, and absence of lamellar structure as the ultimate structure. Such change of microphase segregation pattern in AB diblock copolymer at constant temperature is described mainly from the volume balance between A- and B-segments connecting at the interface.[20,21,28] Then, due to highly hydrated nature, PEG segments tend to take expanded conformation in water. Alternatively, PIC phase tends to decrease interfacial area because of decreased ion osmotic pressure and dehydrated nature of charge-neutralized PIC strands. Spherical micelles were formed at PICs with $f_{PEG}$ 11.1% and 12.1%, presumably relying on larger fraction of PEG part compared to that of PIC part.[12,13,18,19] By decreasing $f_{PEG,}$ or the replacement of PEG−PAsp with homo-PAsp, the number of PEG chains at the interface between PIC part and PEG part decrease, while relative volume for PIC part increase. Probably, this change in the balance resulted in the variation of PIC nanostructure from spherical to cylindrical micelles, and then to growth for the cylindrical or planar PIC network.

**3.2. The Influence of Temperature on PIC Nanoarchitectures.** At room temperature, PEG strands tend to take their swollen state in water with high excluded volume due to its favorable interaction with water. This tendency was reflected by polymer−solvent or Flory−Huggins interaction parameter ($\chi$) for PEG in water (0.41−0.45),[29−31] which is lower than 0.50, and positive value of their second virial coefficient ($A_2$).[29−34] It is interesting to note that PEG inherently exhibited dehydrated behavior by increasing in temperature,[29−36] thus the volume balance between PEG part respect to PIC part can be modulated by temperature. In this context, PIC structure was examined at various preparation and incubation temperatures (25−70 °C). Remarkably, substantial morphological change was observed by increasing incubation temperature for PICs prepared above $f_{PEG}$ of 8.8% (Figures 1a−c, 2a,b, and 3a−o). Increase in temperature induced variety of morphological transition of PICs: the originally observed "spherical micelles" at $f_{PEG}$ = 12.1% at 25 °C was changed to the "connected-cylinder network" at higher tempearture; the "spherical and cylindrical micelles" at $f_{PEG}$ = 11.1% and 10.0% was changed to the "connected-cylinder network", and admirably to the "well-aligned lamellar"; the "connected-cylinder network" at $f_{PEG}$ = 9.4% was also ultimately to the "well-aligned lamellar"; and the "connected-cylinder network" at $f_{PEG}$ = 8.8% was to the "connected-plane network". While at $f_{PEG}$ composition 7.7% and 6.5%, significant morphological change was not observed by increasing temperature, instead the network textures tend to take more densely packed network structures (Figures 2c,d and 3p−u). Overall, the order of PIC structural change by increasing temperature presented similar trend with lowering $f_{PEG}$, but the transition seemed somewhat much more facilitated. This may be reasonable because increasing temperature led to decreasing PEG occupying volume in water, which is signaled by decrement of their hydrodynamic volume,[32] hydrodynamic expansion factor ($a_h$),[32] $A_2$ value[31−33] and increment of $\chi$ value[31,35] of PEG in water as temperature is raised, thus essentially resulting the same effect of decreased $f_{PEG}$. Concomitantly, this suggests the balance of PEG part and PIC part substantially contributed in determining microphase segregation pattern. Yet, the most


dx.doi.org/10.1021/ma500314d | Macromolecules XXXX, XXX, XXX−XXX

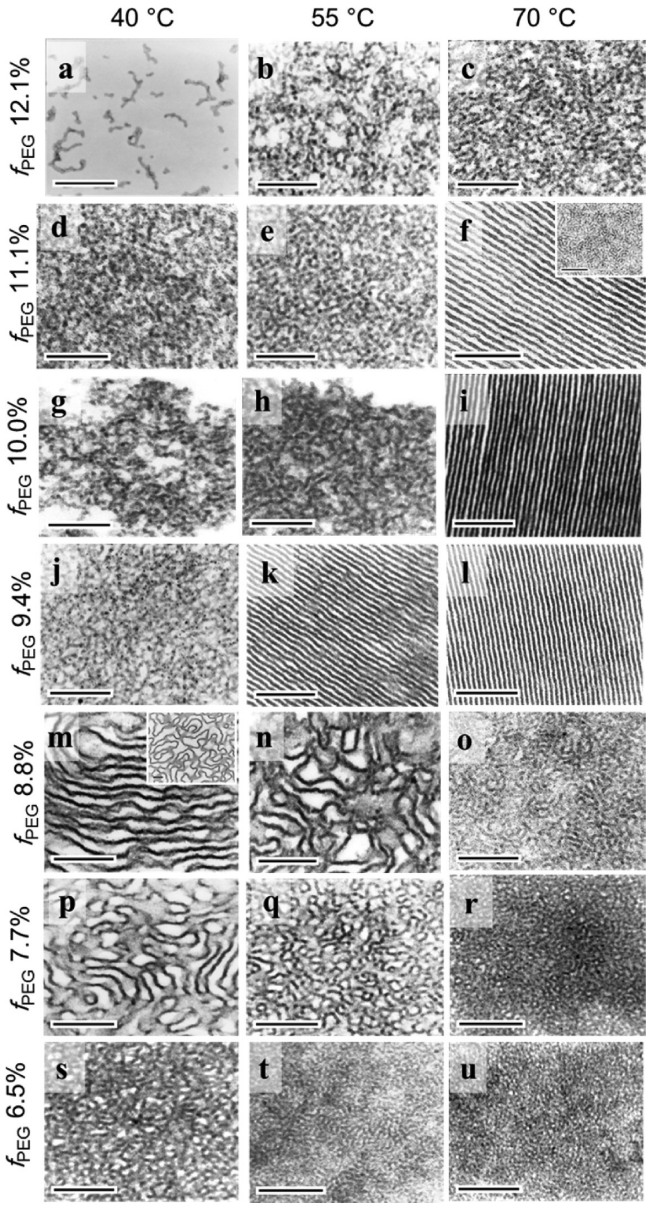


**Figure 3.** Cross section TEM images of PICs prepared at different incubation temperatures (40 °C, 55 and 70 °C). Inset of part f showed coexistence of well-aligned lamellae and network architectures in the same sample, while inset of 3-m showed variation in pore size between the core and the edge of connected-plane network in the same sample. Scale bars represent 250 nm.

fascinating finding upon temperature modulation was the observation of "well-aligned lamellar structure" with PIC thickness of ~11 nm and spacing between PIC of ~12 nm (Table 2) at high temperature with $f_{PEG}$ composition 9.4% - 11.1% (Figure 3f,i,k,l) because the lamellar was the missing structure in the series of morphological change with $f_{PEG}$ at ambient temperature, and to the best of our knowledge, this is the first direct observation of clear alternating lamellar structure of PIC in water from block ionomers. As aforementioned, PIC thickness of ~11 nm is consistent with the thickness of PIC lamellar found in the unilamellar PIC vesicles (10–15 nm),[16] and might be acceptable to assume the observed PIC plane is consisted of unilamellar of PIC based on above calculation of the length of constituent polyelectrolytes in fully extended confirmation. It is worthwhile to notice the formation of well-

**Table 2. Average PIC Thickness and Spacing between PIC Layer of Well-Aligned Lamellae Structure Prepared at Incubation Temperature 55 and 70 °C and Polymer Concentration 1 mg/mL[a]**

| $f_{PEG}$ (%) | temperature (°C) | average spacing between PIC layer (nm) | average PIC thickness (nm) |
|---|---|---|---|
| 10.0 | 70 | 11.8 ± 1.3 | 11.3 ± 1.6 |
| 9.4 | 55 | 12.3 ± 1.4 | 11.0 ± 1.3 |
| 9.4 | 70 | 11.6 ± 1.8 | 11.5 ± 1.4 |

[a]PIC thickness and spacing between PIC layer of coexistence of well-aligned lamellar and network architectures obtained at $f_{PEG}$ 11.1% after being incubated at 70 °C was not shown for clarity.

aligned lamellar structure suggests presence of attraction force between each lamella for the association. Most likely, interaction between PEG segments and water decrease at higher temperature, which is indicated by decreasing $A_2$ value[31−33] and increasing $\chi$ value[31,35] of PEG in water at elevated temperature, and hydrophobic attractive force between PEG layers may have developed because PEG chains shift to hydrophobic nature with elevating temperature. The analysis of the lamellar spacing from TEM images may support this assumption. Theoretically, the end-to-end distance of PEG strands with molecular weight of 2.1k are 16.8 nm and 8.6–9.6 nm for a zigzag and meander model respectively,[37] and 3.5 nm for a random coil model based on Flory's theory. Therefore, the spacing between PIC layers measured to be 12 nm (Table 2) was consistent for PEG to occupy the spacing in well-aligned lamellae structure. Alternatively, at room temperature, PEG is in fully hydrated state with large exclusion volume, thereby no significant attractive force develops to associate each PEG layer. Accordingly, excess water could penetrate into the connected cylinder network or connected plane network to form water channel, so that the mesoporous structures as typically seen in 3D-TEM images might be formed (Figure 2).

It is noteworthy that the thermal behavior of PIC structure was basically reversible. Taking PICs with $f_{PEG}$ 10% as example, reversible transformation of PIC nanoarchitectures was observed for the sample experienced the temperature cycle at 40 and 70 °C, at least for two times. Connected-cylinder PIC network that were observed at PICs incubated at 40 °C (Figure 3g) was changed to well-aligned lamellae by increasing incubation temperature at 70 °C (Figure 4a). These PIC nanoarchitectures were observed again by repeating the incubation temperature cycle at 40 °C (connected-cylinder PIC network; Figure 4b) and 70 °C (well-aligned lamellae; Figure 4c). This result suggested the reversible behavior of PICs in thermal treatment.

The morphological variation found in the PIC system, presenting similar behavior with the well-studied microphase separation found in other block copolymer system, could be submitted as new system to construct nanoarchitectures by self-assembly in water and also would stimulate study to depict a general rule governing structural formation in the self-assembly process. Further, the nanoarchitectures settled in the bulk PICs, featured as mesoporous materials with water channel, presents significant capacity in loading materials within their large inner space. Also the space may serve as nanoreaction field with confined space. Finally, the facile preparation of the mesoporous PICs in water without using sacrificial materials or templates should also be highlighted as distinguished feature


dx.doi.org/10.1021/ma500314d | Macromolecules XXXX, XXX, XXX–XXX

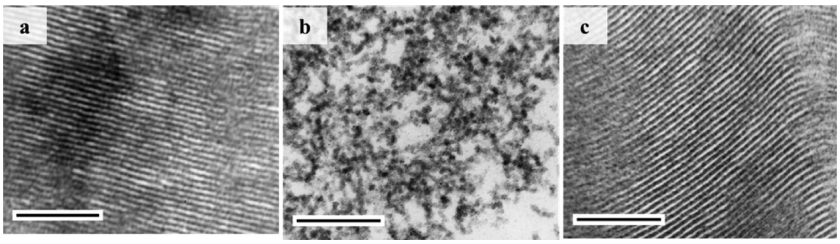


**Figure 4.** Cross section TEM images of PICs with $f_{PEG}$ 10% and polymer concentration 1 mg/mL incubated at (a) 70 °C of first cycle; (b) 40 °C of second cycle; (c) 70 °C of second cycle. Scale bars represent 250 nm.

upon further extending this PIC system for practical application.

## 4. CONCLUSION

Upon modulating $f_{PEG}$ and temperature, we finally observed significant morphology transition of PIC parts, namely sphere, cylinder, connected cylinder, connected plane, and lamella as of particular interest, which follows the well-documented microphase segregation pattern modeled for AB diblock copolymer system. Considering this analogy of PICs and the general microphase segregation pattern, the characteristic structures of connected-cylinder network and connected-plane network found in the PIC system were consistent with bicontinuous phase, which appears between cylinder and lamella, yet further detailed study is needed to verify this speculation. To the best of our knowledge, this is the first report of this series morphological changes occurring in the PIC system in aqueous medium with thermal reversibility, and thus a currently intensive study is ongoing to fully explore this unique architecture with an anticipation to open a new category of self-assembled nanoarchitectures by PICs.

## ■ ASSOCIATED CONTENT

### Ⓢ Supporting Information

DLS results, electrical sensing zone results, optical microscopic observations (DFM and PCM observations), snapshot from each 3D TEM tomography movies, and 3D TEM tomography movies. This material is available free of charge via the Internet at http://pubs.acs.org.

## ■ AUTHOR INFORMATION

### Corresponding Authors

*(A.K.) E-mail: kishimura@mail.cstm.kyushu-u.ac.jp.
*(K.K.) E-mail: kataoka@bmw.t.u-tokyo.ac.jp.

### Author Contributions

[§]These two authors contributed equally

### Notes

The authors declare no competing financial interest.

## ■ ACKNOWLEDGMENTS

This research was supported in part by a Grant-in-Aid for Scientific Research (No. 21106505 and 23106705 to A.K.) from the Ministry of Education, Culture, Sports, Science, and Technology (MEXT) of Japan, Grant-in-Aid for Specially Promoted Research and Core to Core Program for A. Advanced Research Networks, the Center of Innovation (COI) Program and Precursory Research for Embryonic Science and Technology (PRESTO) from Japan Science and Technology Agency (JST), Funding Program for World-Leading Innovative R&D on Science and Technology (FIRST Program) from the Japan Society for the Promotion of Science (JSPS). We thank Dr. Satoru Fukuda from the University of Tokyo Hospital for TEM sample preparation, and Mr. Hashime Hoshi from JEOL Ltd. for his valuable support in conducting 3-D TEM tomography measurements that were conducted in Research Hub for Advanced Nano Characterization, The University of Tokyo, supported by the Ministry of Education, Culture, Sports, Science and Technology (MEXT) of Japan. A. K. thanks the Ogasawara Foundation for the Promotion of Science & Engineering for financial support. A.W. is very grateful for the fellowship from MEXT of Japan and Grants for Excellent Graduate Schools "Medical System Innovation through Multidisciplinary Integration", The University of Tokyo.

## ■ REFERENCES

(1) Scacher, F. H.; Rupar, P. A.; Manners, I. *Angew. Chem., Int. Ed.* **2012**, *51*, 7898−7921.
(2) Mai, Y.; Eisenberg, A. *Chem. Soc. Rev.* **2012**, *41*, 5969−5985.
(3) Tseng, Y.-C.; Darling, S. B. *Polymers* **2010**, *2*, 470−489.
(4) Bang, J.; Jeong, U.; Ryu, D. Y.; Russells, T. P.; Hawker, C. J. *Adv. Mater.* **2009**, *21*, 4769−4792.
(5) Kabanov, A. V.; Kabanov, V. A. *Adv. Drug. Delivery Rev.* **1998**, *30*, 49−60.
(6) Thünemann, A. F.; Müller, M.; Dautzenberg, H.; Joanny, J. F.; Löwen, H. *Adv. Polym. Sci.* **2004**, *166*, 113−171.
(7) Altunbas, A.; Lee, S. J.; Rajasekaran, S. A.; Schneider, J. P.; Pochan, D. J. *Biomaterials* **2011**, *32*, 5906−5914.
(8) Holowka, E. P.; Pochan, D. J.; Deming, T. J. *J. Am. Chem. Soc.* **2005**, *127*, 12423−12428.
(9) Schatz, C.; Domard, A.; Viton, C.; Pichot, C.; Delair, T. *Biomacromolecules* **2004**, *5*, 1882−1892.
(10) Wen, Y.; Grøndahl, L.; Gallego, M. R.; Jorgensen, L.; Møller, E. H.; Nielsen, H. M. *Biomacromolecules* **2012**, *13*, 905−917.
(11) Boddohi, S.; Moore, N.; Johnson, P. A.; Kipper, M. J. *Biomacromolecules* **2009**, *10*, 1402−1409.
(12) Kataoka, K.; Harada, A.; Nagasaki, Y. *Adv. Drug. Delivery Rev.* **2001**, *47*, 113−131.
(13) Lee, Y.; Kataoka, K. *Soft Matter* **2009**, *5*, 3810−3817.
(14) Harada, A.; Kataoka, K. *Macromolecules* **1995**, *28*, 5294−5299.
(15) Koide, A.; Kishimura, A.; Osada, K.; Jang, W.-D.; Yamasaki, Y.; Kataoka, K. *J. Am. Chem. Soc.* **2006**, *128*, 5988−5989.
(16) Anraku, Y.; Kishimura, A.; Oba, M.; Yamasaki, Y.; Kataoka, K. *J. Am. Chem. Soc.* **2010**, *132*, 1631−1636.
(17) Kishimura, A. *Polym. J.* **2013**, *45*, 892−897.
(18) Dong, W.-F.; Kishimura, A.; Anraku, Y.; Chuanoi, S.; Yamasaki, Y.; Kataoka, K. *J. Am. Chem. Soc.* **2009**, *131*, 3804−3805.
(19) Chuanoi, S.; Kishimura, A.; Dong, W.-F.; Anraku, Y.; Yamasaki, Y.; Kataoka, K. *Polym. J.* **2014**, *46*, 130−135.
(20) Bates, F. S. *Science* **1991**, *251*, 898−905.
(21) Bates, F. S.; Fredrickson, G. H. *Annu. Rev. Phys. Chem.* **1990**, *41*, 525−557.
(22) Maunsbach, A. B. In *Cell Biology: A Laboratory Handbook*, 3rd ed.; Celis, J. E., Ed.; Elsevier Inc.: Amsterdam, 2006; pp 221−231.

(23) Sabatini, D. D.; Bensch, K.; Barrnett, R. J. *J. Cell. Biol.* **1963**, *17*, 19−58.
(24) Doughty, M. J.; Bergmanson, J. P. G.; Blocker, Y. *Tissue Cell* **1997**, *29*, 533−547.
(25) Guerrero, F.; Cerutti, P.; Marcaccini, A. *Int. J. Morphol.* **2011**, *29*, 656−660.
(26) Guisan, J. M.; Fernandez-Lafuente, R. *Biomacromolecules* **2006**, *7*, 2610−2615.
(27) Migneault, I.; Dartiguenave, C.; Bertrand, M. J.; Waldron, K. C. *Biotechniques* **2004**, *37*, 790−802.
(28) Sugihara, S.; Blanazs, A.; Armes, S. P.; Ryan, A. J.; Lewis, A. L. *J. Am. Chem. Soc.* **2011**, *133*, 15707−15713.
(29) Lee, J. H.; Lee, H. B.; Andrade, J. D. *Prog. Polym. Sci.* **1995**, *20*, 1043−1079.
(30) Yuan, Q. W. In *Polymer Data Handbook*; Mark, J. E., Ed.; Oxford University Press: New York, 1999; pp 542−552.
(31) Dormidontova, E. E. *Macromolecules* **2002**, *35*, 987−1001.
(32) Dinc, C. O.; Kibarer, G.; Guner, A. *J. Appl. Polym. Sci.* **2010**, *117*, 1100−1119.
(33) Polik, W. F.; Burchard, W. *Macromolecules* **1983**, *16*, 978−982.
(34) Allen, C.; Dos Santos, N.; Gallagher, R.; Chiu, G. N. C.; Shu, Y.; Li, W. M.; Johnstone, S. A.; Janoff, A. S.; Mayer, L. D.; Webb, M. S.; Bally, M. B. *Biosci. Rep.* **2002**, *22*, 225−250.
(35) Eliassi, A.; Modarres, H.; Mansoori, G. A. *J. Chem. Eng. Data* **1999**, *44*, 52−55.
(36) Aseyev, V.; Tenhu, H.; Winnik, F. M. *Adv. Polym. Sci.* **2011**, *242*, 29−89.
(37) Tanford, C.; Nozaki, Y.; Rohde, M. F. *J. Phys. Chem.* **1977**, *81*, 1555−1560.